



*Research article*

## **A preliminary study of porous ceramics with carbon black contents**

**Mohamed Lokman Jalaluddin<sup>1</sup>, Umar Al-Amani Azlan<sup>2,\*</sup> and Mohd Warikh Abd Rashid<sup>1</sup>**

<sup>1</sup> Department of Manufacturing Engineering, Faculty of Manufacturing Engineering, Universiti Teknikal Malaysia Melaka, Malaysia

<sup>2</sup> Department of Industrial Technology, Faculty of Mechanical and Manufacturing Engineering Technology, Universiti Teknikal Malaysia Melaka, Malaysia

\* **Correspondence:** Email: [umar@utem.edu.my](mailto:umar@utem.edu.my); Tel: +6-06-270-4020; Fax: +6-06-270-1065.

**Abstract:** This paper is a study of porous ceramics from a mixture of clay (kaolinite), silica (silicon dioxide), and feldspar by adding the carbon black (CB) with different contents. The results were presented in terms of apparent porosity, relative density, microstructure and porous characteristic, flexural strength and phase formation. As observed, the sintering at 1200 °C is the optimum temperature in this work. In comparison to the samples without CB content, the apparent porosity and relative density of ceramics are highly dependent on the CB contents. This might be attributed to the presence of porous structure as seen in SEM images on the fracture surface of ceramics. It also revealed that the addition of CB resulted in smaller pore sizes and a more uniform pore distribution. The creation of pores in porous ceramics was mainly attributed to the loss of shape of CB microspheres at high temperatures, as observed from SEM. The flexural strength of the sintered samples exhibited an average decrease from 60 to 55 MPa due to the presence of CB, which is typically known to reduce the mechanical properties with high porosity. In XRD results, the muscovite phase is represented by a few of peaks with significant intensities, while the rest peaks are of undetermined phase. The strongest peak at a 26° of 2θ angle, suggesting the presence of potassium and aluminium in the form of silicate minerals.

**Keywords:** ceramics; carbon black; porous structure

---

## 1. Introduction

Energy conservation in structural applications is a significant concern worldwide, including in Malaysia, due to its impact on the environment. To maintain a comfortable indoor environment, air conditioning systems are commonly installed in buildings, which consume a large amount of energy. To reduce energy consumption, it is necessary to limit the absorption of the outside atmosphere, which may have different thermal characteristics than what is required. Ceramic tiles are a popular choice for flooring, walls, roofs, and tables due to their desirable features such as dimensional stability, aesthetics, water resistance, hardness, weight-bearing capacity, abrasion resistance, and ability to withstand temperature changes, shocks, frost, and impact.

Structural ceramics usually consider porosity a defect since it impacts material strength due to the concentration of stress around the pores. Nevertheless, porous ceramics are attractive for several applications due to their large specific surface area, high permeability, low thermal conductivity, and low density. These applications include molten material filtration [1], catalyst support for biomaterials [2], thermal insulation [3], lightweight components [4], and others. To fulfill the requirements of the specific application, it is crucial to manufacture porous ceramics with a controlled pore size and structure.

Regrettably, the brittleness that is intrinsic to ceramics limits their mechanical durability, which poses a significant challenge for extensive engineering applications. To address this issue, pores are incorporated into the ceramic structure. Interestingly, porous ceramics offer a distinct combination of properties that significantly broaden their utility. These properties include characteristics that are similar to their solid counterparts, such as low density, a large specific surface area, high hardness, excellent thermal shock resistance, superior thermal insulation performance, and a low dielectric constant. These properties create new possibilities for numerous applications and various industrial operations.

The classification of porous ceramics has historically been based on their porous structure, which divides them into three types: macro-porosity ( $d > 50$  nm), meso-porosity ( $2$  nm  $< d < 50$  nm), and micro-porosity ( $d < 2$  nm) [5]. However, a commonly used hierarchical porous structure refers to the existence of various pore sizes within a single monolithic matrix. Additionally, porous ceramics can be classified as open-cell or closed-cell based on their fundamental pore structure, which plays a crucial role in defining the suitability of different materials for specific applications [6]. For instance, open-cell designs with interconnected pores are beneficial for fluid transport applications because of their permeability to gases and liquids, while a closed-cell structure with isolated pores within a constant ceramic matrix may be advantageous for insulation applications where fluid movement needs to be regulated [7]. These fundamental structural characteristics effectively determine the resulting mechanical properties and expanded applicability of porous ceramics.

Carbon black (CB) is an industrial material consisting of a fine black powder of almost pure elemental carbon that has been used for centuries [8]. The material is composed of carbon atoms, which are mostly spherical and linked together in aggregates, accounting for over 90% of its composition [9]. The particle size of carbon black ranges from 10 to 500 nm, with larger particle sizes indicating a stronger graphitic structure [10]. Its microstructure, as seen through TEM, is partially onion-like and graphite in nature [9]. CB does not retain impurities after being burned at high temperatures. However, its extraction and usage are hazardous due to its dependence on hydrocarbon degradation [8]. As a result, carbon black is used as a pore-forming agent in the ceramic tile's body composition to control

pore formation. CB is used as a pore-forming agent by putting carbon black particles into the matrix of the material and then withdrawing them to generate holes or pores in the structure. Based on previous study shows that as-prepared porous carbon-based adsorbents (PCBAs) has a more wrinkled and looser surface morphology, and the specific surface area, micropore ratio, and degree of graphitization exhibit an explosive change pattern with increasing pore creation temperature. Whereas raising the pore formation temperature has no effect on the surface chemical characteristics of PCBAs, it can considerably improve the microporosity and surface area of PCBAs. PCBAs with a high microporous ratio and a particular surface area can provide additional sites of activity for toluene adsorption, enhancing their toluene adsorption efficacy [11].

The need for energy conservation in structural applications is currently a pressing issue with a significant impact on the environment globally, including Malaysia. A critical challenge in achieving energy savings is the convective heat loss caused by the use of traditional solid construction materials. Ceramic materials possess thermal properties, including heat capacity and thermal expansion coefficients that affect their ability to store or transfer thermal energy. Heat capacity is a measure of a material's ability to absorb heat from its surroundings, which explains why ceramic surfaces exposed to solar radiation in outdoor conditions often reach high temperatures [12].

The addition of a pore-forming agent can be used to control the porosity of ceramic tiles, which results in a reduction in thermal conductivity. However, the presence of pores can decrease the overall mechanical strength of the material. To maintain the mechanical strength of thermally conductive ceramics, pore-forming agents have been utilized, resulting in a significant increase in porosity. During the heating process, organic particles are burned away, creating holes in the ceramic body. The shape and size of these pores are determined by the type and quantity of pore-forming agent used [13].

The use of CB as a pore-forming agent is intended in the research. The unique characteristics of CB, such as its nanoscale particle size and spherical shape, make it stand out from other conventional pore-forming agents. Furthermore, CB leaves no contaminants after being burned at high temperatures. CB exhibits higher thermal resistance compared to polymethyl methacrylate (PMMA), making it suitable for applications involving elevated temperatures during ceramic processing. Unlike polypropylene (PP) and polymethyl methacrylate (PMMA), CB typically leaves fewer residues during the firing process, resulting in cleaner and more uniform porous ceramics. Lastly, the CB is from ceramic base while PP and PMMA are from polymer base. So that, carbon black is better to use as pore forming agents. The primary objective of this study is to assess the effectiveness of ceramics under various conditions using CB pore-forming agents.

The aims of this investigation include identifying the most suitable amount of CB for creating porous ceramics with preferred traits like porosity, strength, and thermal conductivity. Additionally, analyzing the impact of CB quantity on the microstructure and morphology of porous ceramics, such as pore size distribution, pore connectivity, and grain size. Moreover, examining how CB quantity influences the mechanical properties of porous ceramics, including compressive strength, fracture toughness, and hardness.

## 2. Materials and methods

### 2.1. Materials

To produce the ceramic sample, a mixture of clay (kaolinite), silica (silicon dioxide), and feldspar was employed, with microcline as the resultant mixture. This ceramic blend is porous and has the chemical formula  $\text{Al}_2\text{Si}_2\text{O}_5(\text{OH})_4 + \text{SiO}_2 + \text{KAlSi}_3\text{O}_8$ . The overall weight of the mixture is 310 g, and the weight of each constituent can be calculated by using a chemical equation. Besides, the quantities for clay, feldspar, and silica are 24.84, 40.64, and 4.51 g, respectively.

### 2.2. Sample preparation

The production of ceramic structure samples involved the use of both disc and bar shapes. The bar-shaped samples had an average length of 75 mm, a width of 10 mm, and a height of 5 mm, while the disc-shaped samples had a diameter of 5 mm. Four different ceramic mixtures were prepared, with proportions of 0%, 3%, 5%, and 10%, using a total of 70 g of materials. The clay and feldspar components were in solid form and were ground using a mortar and pestle, while silica was in powder form. Each mixture was used to produce seven sintered samples, resulting in a total of 34 sintered ceramic samples. To conduct the tests, 10 pieces were produced for each mixture ratio. The weight of each raw ingredient powder was determined to ensure that the porous ceramic composition contained a uniform percentage of raw powder in each sample. Following this, the composition was supplemented with the porous ceramic agent, at rates of 0%, 3%, 5%, and 10%.

In order to create a strong and durable ceramic sample, a process called sintering was employed. This is a crucial step in producing a porous ceramic material that is highly compacted. In this study, the powder mixture was partially sintered by heating it to 1200 °C, based on a single ramp-up temperature curve. The temperature was increased gradually, at a rate of 5 °C/min, until it reached the desired sintering temperature. Once this was achieved, the material was left to cool naturally to room temperature, which is typically around 25–28 °C. Prior to consolidation of the powder, the material was preheated, which caused it to oxidize and prevented it from bursting out of the structure.

As mentioned earlier, the ceramic samples were fabricated in both bar and disc shapes. The bar shape was preferred as it could uniformly compact the powder under a uniaxial load, and its dimensions averaged 75 mm in length, 10 mm in width, and 5 mm in height. Compared to the square tile form, this shape required a minimal amount of material. The SM100-Universal Test Machine was employed to produce the porous ceramic structure in this process. Initially, the porous ceramic powder was added to both the disc and bar-shaped moulds, and low pressure was applied to the plunger to form the first compact. Subsequently, the mould was placed in the Universal Test Machine, and a pressure of 20 MPa was applied for 60 s. This process resulted in the formation of a bar or disc-shaped structure with adequate force. These findings highlight that dry pressing is a crucial step in determining the force exerted on the sample.

### 2.3. Materials characterization

The performance of the porous ceramic materials was assessed based on parameters such as porosity, density, and mechanical properties, including strength. The investigation also involved

conducting flexural strength tests and utilizing scanning electron microscopy (SEM). To evaluate the characteristics of the porous ceramic, CB was utilized at varying concentrations of 0%, 3%, 5%, and 10%. In each group, there was 3 samples were made.

Archimedes' principle states that the buoyant force exerted on a submerged object is equivalent to the weight of the fluid displaced by the object. In this study, the Archimedes buoyancy technique was employed to calculate the apparent porosity and density. The dry mass was represented by  $W_a$ , the mass suspended in water by  $W_b$  and the saturated mass by  $W_c$ . In order to determine the apparent porosity and density formula, the  $W_a$  of the samples was accurately measured using a precision balance A&D FZ-300i-EC after being heated. Following this, the samples were immersed in distilled water for a brief period and the  $W_b$  and  $W_c$  were measured utilizing the same scale. The obtained data was analysed to determine the apparent porosity and density formula.

SEM is a sophisticated method for capturing images of material microstructures, which is typically carried out under a vacuum environment. This is due to the possibility of gas molecules interfering with the electron beam and the secondary and backscattered electrons that are required for imaging purposes. To analyze the samples in this study, microstructure images were taken with the help of a JEOL JSM-6010PLUS/LV instrument.

The testing in this study involved examining the top surface and cross-section samples, which required several preparation steps such as grinding, polishing, and thermal etching prior to SEM analysis. To grind each sample, 1000, 1500, and 2000 grit sizes were used. The grinding process was conducted in accordance with the grit size of adhesive paper to ensure that the sample surface was free of scratches. A brief grinding period was carried out for each sample. After grinding, the samples were polished with a micro pad and 0.05  $\mu\text{m}$  of  $\text{Al}_2\text{O}_3$ .

After the grinding and polishing were finished, the samples were dried in an oven at 60 °C for less than a minute. Once dried, all samples underwent a thermal etching process by soaking them for one minute at a temperature of 1100 °C. Before being scanned, the samples needed to be dried and cleaned. To mount the samples, an adhesive tab was attached to the aluminium stub. The vacuum chamber was vented using the venting process. The samples were then placed in the sample holder and the chamber door was closed. The pump was left running until it reached its maximum vacuum level. Once this was achieved, the samples were ready for testing.

The flexural test, also referred to as the bending tensile test, is a technique for measuring the flexural strength and other important characteristics of materials. This destructive material testing approach is used for plastics, fibre-reinforced plastics (FRP), metals, and ceramics. The procedure for conducting flexural tests is similar across different materials. A 3-point flexural test was utilized in this instance, although the number of pressure points and sample support may vary.

Standardized cylindrical samples were placed at the center of the inspection fixture for flexural testing. The rounded support rollers, also known as bearings, were positioned at a specific distance from each other, which was known as the support width. The diameter of the cylindrical sample was directly proportional to the support width of the bearings. A gradually increasing force was applied to the sample until it broke or reached the predetermined deformation point set by the testing punch, which descended gently and at a consistent speed. The maximum load applied during the flexural test was known as the breaking force.

Finally, the sintered samples with different CB contents were also sent to the X-ray diffraction (XRD) machine (PANalytical X'Pert PRO). The XRD analysis was used to determine the crystalline phases present in a material and, as a result, to reveal information about its chemical composition.

### 3. Results and discussion

#### 3.1. Optimizing the sintering temperatures

The temperature required to heat the samples was not initially determined due to variations in the melting points of the raw materials used. As a result, the samples were subjected to a temperature of 1075 °C in a furnace, but this was unsuccessful as the surface of the sample became powdery. Moreover, the unsuitable temperature condition weakened the structure of the sample, making it prone to breakage. To address this issue, the temperature was increased to 1250 °C. As shown in Table 1, the shape of the sample changed from disc to oval, but the surface was smooth and shiny in comparison to samples burnt at lower temperatures. The sample without CB was used as a reference for sintering the other samples containing CB.





One of the noticeable differences observed in samples burnt at various temperatures is the change in their dimensions, including diameter, thickness, and shape. With an increase in the sintering temperature, the samples exhibited a shrinking effect. Based on Table 1, the diameter of the sample subjected to a temperature of 1075 °C is 12.42 mm, while that of the sample burnt at 1250 °C is 7.65 mm. This indicates a decrease of 38% in the firing shrinkage of the diameter length as compared to the sample sintered at 1075 °C. The sample undergoes shrinkage due to various factors.

Based on the previous research, the results show that the sintering temperature has a significant effect on the properties of the ceramic tiles. At low temperatures which are less than 1100 °C, the tiles did not achieve sufficient density, resulting in a powdery surface and weak structure. As the temperature increased, the density of the tiles improved, and their mechanical strength increased. However, at higher temperatures which are above 1250 °C, the tiles exhibited excessive shrinkage and deformation, which could compromise their dimensional accuracy and overall quality. The optimum sintering temperature was found to be 1200 °C, which resulted in tiles with a high density, good mechanical strength, and minimal shrinkage [14].

The water present in the clay particles includes both residual moisture and chemically-bound water. As the clay is fired, the water that is chemically bound to the clay particles is expelled, while any residual moisture evaporates. This drying process leads to a reduction in the size of the clay, also known as shrinkage. The shrinkage is caused by both chemical and physical changes, such as the burning off of organic matter during the firing process, which leads to a reduction in the clay's volume. Additionally, the clay undergoes vitrification during the firing process, contributing to the overall shrinkage.

According to Table 1, the weight of the sample burned at 1075 °C was 0.842 g, while the weight of the sample burned at 1250 °C was 0.747 g. This represents an 11% decrease in sample weight during sintering when compared to the sample sintered at 1075 °C. The sample underwent several factors that contributed to its shrinkage. Weight changes were mainly caused by the vaporization of water and carbon dioxide from the raw materials. Evaporation of water was responsible for most of the weight loss in samples heated to temperatures up to 600 °C, but at temperatures above 600 °C, weight loss resulted from both evaporation and the breakdown of the material's constituents [15].

**Table 1.** Variations in sintering temperatures resulting in physical alterations in ceramic samples.

No. Sample specification	Before sintering	1075 °C	1200 °C	1250 °C
1. Image				
2. Diameter	13.08 mm (initial)	12.42 mm (-5.05%)	10.70 mm (-18.20%)	7.65 mm (-41.51%)
3. Thickness	4.82 mm (initial)	4.72 mm (-2.07%)	4.10 mm (-14.94%)	5.70 mm (18.26%)
4. Surface	Powdery	Powdery	Not powdery	Not powdery
5. Weight (g)	0.871 (-8.32%)	0.842 (-11.37%)	0.849 (-10.63%)	0.747 (-21.37%)
6. Shape	Disc	Disc	Disc	Oval
7. Remarks	The sample is prone to debris or breakage in powdery condition	The surface of the sample remains dusty and rough	The sample displays a notable level of contraction and a relatively smooth surface	The sample has a highly lustrous appearance but has undergone a change in its original shape

**Table 2.** Alterations in the physical properties of bar-shaped samples.

Percentage of CB	Type of sample	Original size (mm) $l \times w \times h$	Sintered size (mm) $l \times w \times h$	Percentage of shrinking
0%	Sample 1	75 × 10 × 4.8	66.4 × 8.9 × 3.9	-35.98%
	Sample 2	75 × 10 × 4.9	66.5 × 9.0 × 3.8	-38.11%
3%	Sample 1	75 × 10 × 4.7	66.6 × 9.1 × 3.8	-34.67%
	Sample 2	75 × 10 × 4.8	66.3 × 9.0 × 3.9	-35.36%
5%	Sample 1	75 × 10 × 4.8	66.1 × 8.9 × 3.8	-37.90%
	Sample 2	75 × 10 × 4.9	66.1 × 9.0 × 3.8	-38.49%
10%	Sample 1	75 × 10 × 4.8	66.2 × 9.1 × 3.9	-35.98%
	Sample 2	75 × 10 × 4.7	66.0 × 9.2 × 3.9	-32.82%

Table 2 shows that all samples were sintered at 1200 °C in a furnace, and sample 2 containing 5% CB had the highest shrinkage rate at 38.49%. Despite having a lower shrinkage rate of 38.11%, sample 2 with 0% CB still followed closely behind sample 2 with 5% CB. Sample 2 with 10% CB had the lowest shrinkage rate at 32.82%. The reduction in size of the samples was due to various factors. The primary cause was the vaporization of water and carbon dioxide from the raw materials. Furthermore, the sintering process led to an increase in grain size by filling in the pre-existing pores and strengthening the bond between the elements in the samples [16]. The sintering process aims to minimize the surface energy of the components by reducing the vapor-solid interfaces between the particles. This leads to increased density and improved mechanical properties as the pores are reduced or even closed during the diffusion process.

### 3.2. Analysis of the properties of fired ceramics

Each concentration of CB samples, including 0%, 3%, 5%, and 10%, were evaluated twice for  $W_a$ ,  $W_b$ , and  $W_c$ . The sample used to calculate the apparent porosity, where the highest value among all samples tested is 43.75% for 3% of CB according to Figure 1. The apparent porosity for 0% of CB is 16.95%. Although the 5% CB sample decreased to 41.67%, it is still lower than the 3% mark. Similarly, the reading for the apparent porosity percentage decreased to 38.89% in the sample with 10% CB. The amount of CB utilized in the ceramics is one of the elements responsible for the apparent porosity seen in the samples. Referring to Figure 1, it can be observed that the percentage of apparent porosity is at its lowest for 0% of CB but increases significantly to reach its highest value at 3% of CB. However, the apparent porosity was found to be slightly decreased (4.7%–6.7%) as the CB concentration increases.

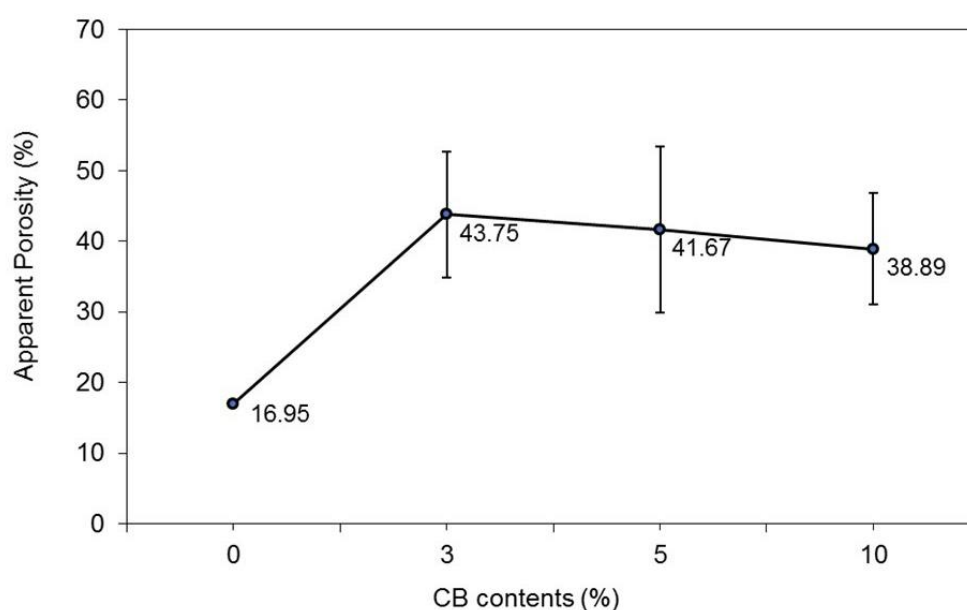


**Figure 1.** Variation in apparent porosity percentage with different CB contents.

Figure 2 also demonstrates that the relative density of 0% of CB is the highest among all samples, but this value decreases proportionally for 3% of CB. On the other hand, samples with 5% and 10% of CB exhibit higher relative density than the sample with 3% of CB. Interestingly, the gradually increase of relative density of the samples with 3% to 10% CB contents was recorded of about 3%–4.5%. This might be attributed to the uniformity of pore sizes in the ceramic samples. It was also then supported by the small difference in the standard deviation for samples with CB contents. It is worth noting that the concentration of CB in the ceramics is a significant factor affecting the apparent porosity and relative density observed in the ceramic samples.



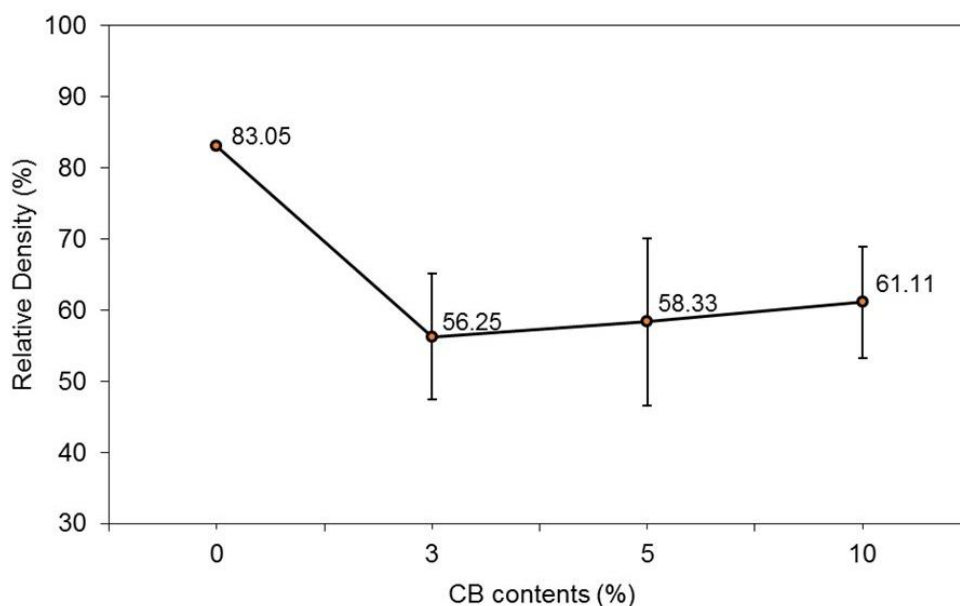
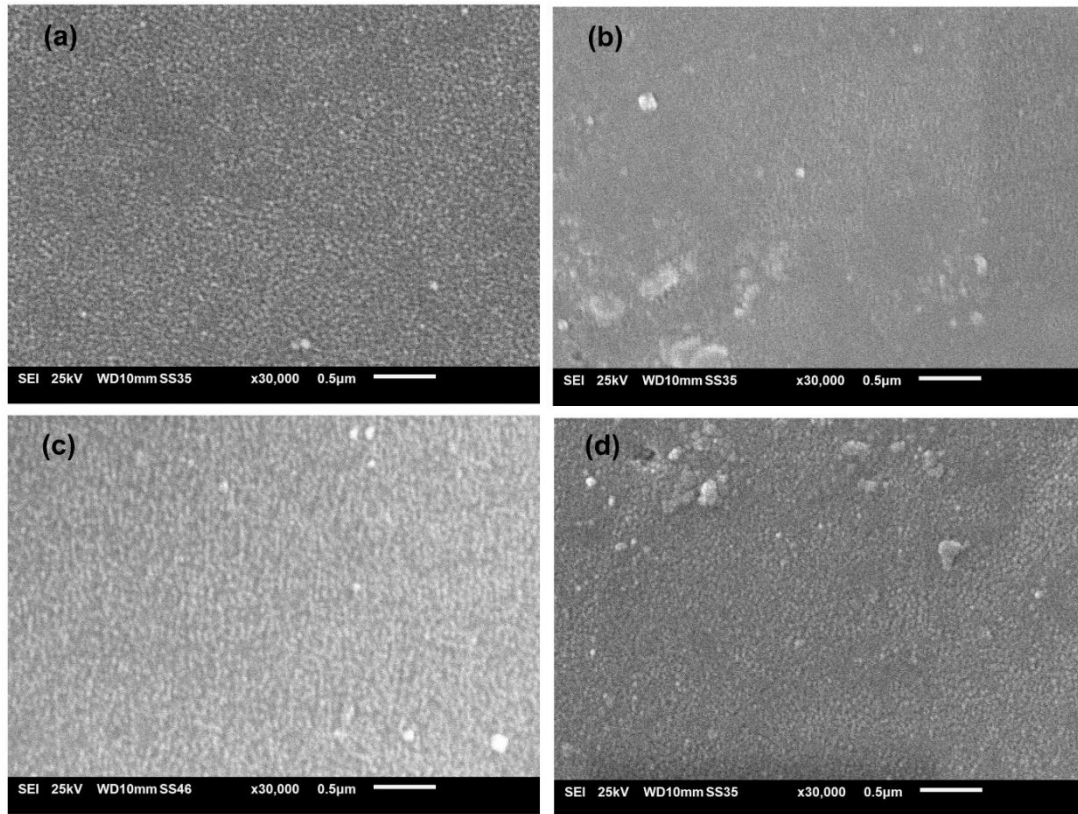


**Figure 2.** Relative density percentages were determined for various concentrations of CB.

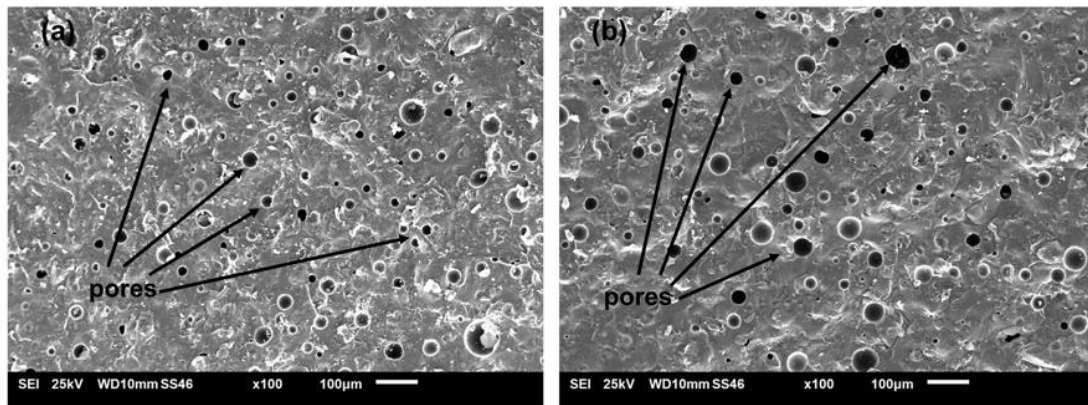
### 3.3. Microstructures of porous ceramics

Figure 3 displays the top surface of sintered samples at 1200 °C with different CB contents. As shown in Figure 3a–d, there were obviously differences in terms of microstructures of the sample without CB content and other samples with CB contents. In Figure 3a, the top surface displays small grains size with magnification of 30 kx. As the increased in the CB contents, the microstructure images were not clearly seen with SEM at the same magnification. This might be the constrain of the SEM machine to observe the top surface of ceramic samples in this work.

In order to study the pore sizes and numbers, the cross section of samples was also observed as shown in Figure 4. In Figure 4a (0% without CB), the sample had a compact structure with a uniform micro-pore distribution and a low porosity level. However, with the addition of 10% more CB, larger pores began to appear in Figure 4b. CB microspheres losing their shape at high temperatures were primarily responsible for creating pores in porous ceramics. Reduced size porogen particles of about less than 100  $\mu\text{m}$  resulted in an increased quantity of minor pores, whereas larger particles resulted in a decreased quantity of larger pores. As the number of CB microspheres increased, the apparent porosity of the material also increased [17,18]. When the addition levels of CB were increased from 0% to 10%, the apparent porosity of porous ceramics increased to over 21%. This suggests that CB can act as pore-forming agents, contributing to high porosity in porous ceramics. Figure 4 demonstrates that the macroscopic structure of the sample remains intact even after the CB microspheres have been burned away [19].



**Figure 3.** SEM images of sintered samples with varying CB contents for (a) 0%, (b) 3%, (c) 5%, and (d) 10%.



**Figure 4.** SEM images depicting the cross-section of sintered samples with various CB contents: (a) 0% and (b) 10%.

### 3.4. Flexural strength of porous ceramics

To evaluate the impact of pore structure on sample strength, a three-point flexural test was carried out. The test was performed using the Shimadzu AG-100kN-X plus machine, capable of handling loads

up to 100 kN, on bars made from sintered samples with porosities ranging from 16% to 43%. The experiment was repeated twice for each CB sample, containing concentrations of 0%, 3%, 5%, and 10% of CB, at a speed of 1 mm/min. Figure 5 displays the flexural strength of sintered samples with and without the addition of CB. The sample without CB exhibited the highest strength of 60.9081 MPa at a temperature of 1200 °C. On the other hand, the strength of sintered samples decreased from an average of 60 to 55 MPa due to the presence of CB contents. As is commonly known, the mechanical properties decrease with increasing porosity [20]. In this case, the sintering process involved the liquid phase sintering method and CB degradation [21], resulting in the breakdown of CB particles above 550 °C, which increased the sample's pore size. As a general rule, a sample's strength decreases as its porosity increases.

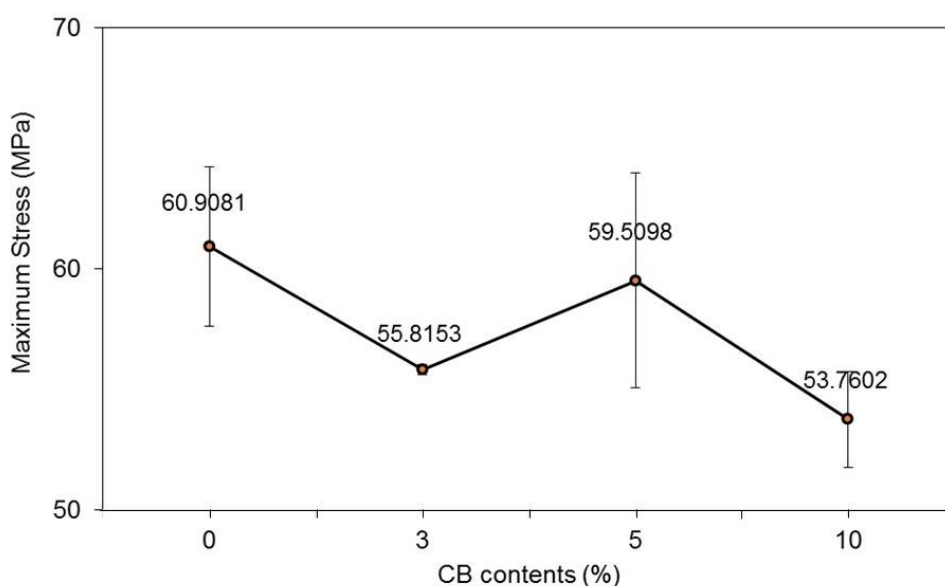


**Figure 5.** The outcome of the flexural strength test conducted on varying proportions of CB.

### 3.5. Phase formation of sintered ceramics

XRD was used to analyze the phase and structure of ceramics. An XRD pattern of porous ceramics made with 0%, 3%, 5% and 10% of CB were depicted. As can be observed, the XRD patterns of common ceramics including kaolinite ( $\text{Al}_2\text{O}_3 \cdot 2\text{Si}_2\text{O}_2 \cdot 2\text{H}_2\text{O}$ ), silica ( $\text{SiO}_2$ ), and feldspar ( $\text{KAlSi}_3\text{O}_8$ ) were easily identifiable. This proves that the primary ceramic structure and phase were successfully created following sintering. However, it was also discovered that a phase with modest peaks and an unknown phase was present. It is thought that the unidentified phase might be the intermediary phase of the particular ceramic component. The peak creation of ceramics with various CB contents is depicted in Figure 6. As can be seen, the muscovite phase is represented by a few of peaks with significant intensities, while the rest peaks are of undetermined phase. The strongest peak can be clearly seen at a  $26^\circ$  of  $2\theta$  angle, suggesting the presence of potassium and aluminium in the form of silicate minerals. Additionally, from samples with 3% CB concentration to those with 10% CB content, the trend of peak formation is relatively constant across all samples. This research demonstrated that peak formation is not much impacted by rising CB concentrations. However, there is a minor difference between samples with and without CB in terms of peak intensity, especially at  $26^\circ$  of  $2\theta$  angle.

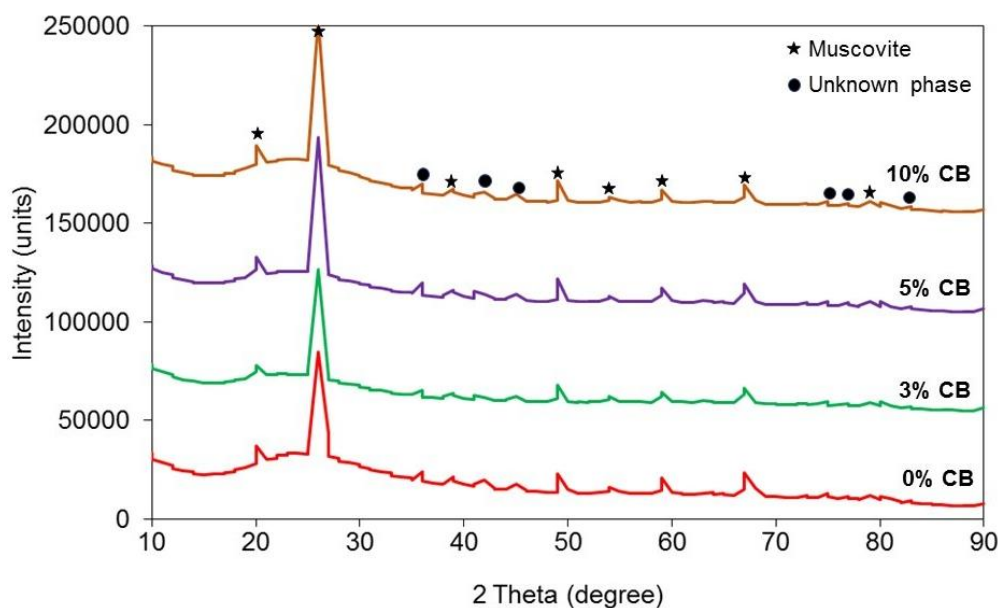


**Figure 6.** XRD patterns of ceramics with different CB contents.

#### 4. Conclusions

In this study, CB was employed as a pore-forming agent (PFA) to fabricate porous ceramics with micro-pores and microstructure. The results revealed that the porosity levels of the ceramics could be easily adjusted by varying the amount of CB. A roughly linear correlation was observed between the amount of CB incorporation and the open porosity of the samples. Furthermore, it was found that CB reduced the number of closed pores and produced more open porosity. The particle size distribution of CB had no effect on the amount of porosity but significantly impacted the number, size, and quantity of pores. The inclusion of CB in the sintered sample resulted in an increased porosity of the ceramics fired at 1200 °C, as compared to those without CB at the same temperature. Moreover, the use of PFA effectively facilitated the formation and augmentation of pores, which was evident from the SEM image of the cross-section of the samples with and without CB. The SEM micrographs show that the pores are relatively uniform in size and distributed evenly throughout the ceramic matrix. The formation of pores in the porous ceramics was mainly attributed to the deformation of CB microspheres at elevated temperatures. The ceramic sample without CB exhibited the highest strength, measuring 60 MPa at 1200 °C. However, the incorporation of CB resulted in a decrease in the sintered samples' strength, which dropped from 59 to 53 MPa depending on the CB percentage. The adverse effect of high porosity on the mechanical properties, such as strength, of the sample is widely acknowledged. Nevertheless, in this study, as the CB was burned off below the sintering temperature, the resulting pores did not have any impact on the tests or results, which was evident in the SEM images. In XRD results, the strongest peak at a 26° of 2θ angle, suggesting the presence of potassium and aluminium in the form of silicate minerals.

## Use of AI tools declaration

The authors declare they have not used Artificial Intelligence (AI) tools in the creation of this article.

## Acknowledgments

The authors extend their appreciation to the Skim Zamalah Universiti Teknikal Malaysia Melaka (UTeM), as well as to UTeM for funding this research work through project number PJP/2020/FTKMP/TD/S01727.

## Conflict of interest

The authors declare that they have no conflict of interest.

## References

1. Taslicukur Z, Balaban C, Kuskonmaz N (2007) Production of ceramic foam filters for molten metal filtration using expanded polystyrene. *J Eur Ceram Soc* 27: 637–640. <https://doi.org/10.1016/j.jeurceramsoc.2006.04.129>
2. Vogt UF, Györfy L, Herzog A, et al. (2007) Macroporous silicon carbide foams for porous burner applications and catalyst supports. *J Phys Chem Solids* 68: 1234–1238. <https://doi.org/10.1016/j.jpcs.2006.12.008>
3. Zhang Y, Wu Y, Yang X, et al. (2020) High-strength thermal insulating mullite nanofibrous porous ceramics. *J Eur Ceram Soc* 40: 2090–2096. <https://doi.org/10.1016/j.jeurceramsoc.2020.01.011>
4. Orlovská M, Chlup Z, Bača Ľ, et al. (2020) Fracture and mechanical properties of lightweight alumina ceramics prepared by fused filament fabrication. *J Eur Ceram Soc* 40: 4837–4843. <https://doi.org/10.1016/j.jeurceramsoc.2020.02.026>
5. Ohji T, Fukushima M (2012) Macro-porous ceramics: Processing and properties. *Int Mater Rev* 57: 115–131. <https://doi.org/10.1179/1743280411Y.0000000006>
6. Twigg MV, Richardson JT (2007) Fundamentals and applications of structured ceramic foam catalysts. *Ind Eng Chem Res* 46: 4166–4177. <https://doi.org/10.1021/ie061122o>
7. Eom JH, Kim YW, Raju S (2013) Processing and properties of macroporous silicon carbide ceramics: A review. *J Asian Ceram Soc* 1: 220–242. <https://doi.org/10.1016/j.jascer.2013.07.003>
8. Tofighy MA, Mohammadi T (2019) Chapter Nine—Barrier, diffusion, and transport properties of rubber nanocomposites containing carbon nanofillers, In: Yaragalla S, Mishra RK, Thomas S, et al., *Carbon-Based Nanofillers and Their Rubber Nanocomposites*, Oxford: Elsevier.
9. Fan Y, Fowler GD, Zhao M (2020) The past, present and future of carbon black as a rubber reinforcing filler—A review. *J Clean Prod* 247: 119115. <https://doi.org/10.1016/j.jclepro.2019.119115>
10. Donnet JB, Bansal RC, Wang MJ (2017) *Carbon Black: Science and Technology*, 2 Eds., New York: Routledge.

11. Chen Y, Fan C, Li X, et al. (2023) Preparation of carbon black-based porous carbon adsorbents and study of toluene adsorption properties. *J Chem Technol Biot* 98: 117–128. <https://doi.org/10.1002/jctb.7220>
12. Živcová Z, Gregorová E, Pabst W, et al. (2009) Thermal conductivity of porous alumina ceramics prepared using starch as a pore-forming agent. *J Eur Ceram Soc* 29: 347–353. <https://doi.org/10.1016/j.jeurceramsoc.2008.06.018>
13. Liu J, Li Y, Li Y, et al. (2016) Effects of pore structure on thermal conductivity and strength of alumina porous ceramics using carbon black as pore-forming agent. *Ceram Int* 42: 8221–8228. <https://doi.org/10.1016/j.ceramint.2016.02.032>
14. Wang W, Sun K, Liu H (2020) Effects of different aluminum sources on morphologies and properties of ceramic floor tiles from red mud. *Constr Build Mater* 241: 118119. <https://doi.org/10.1016/j.conbuildmat.2020.118119>
15. Talaei M, Mostofinejad D (2021) Mechanical properties of fiber-reinforced concrete containing waste porcelain aggregates under elevated temperatures. *Constr Build Mater* 289: 122854. <https://doi.org/10.1016/j.conbuildmat.2021.122854>
16. Anwar MS, Bukhari SZA, Ha JH, et al. (2021) Effect of Ni content and its particle size on electrical resistivity and flexural strength of porous SiC ceramic sintered at low temperature using clay additive. *Ceram Int* 47: 31536–31547. <https://doi.org/10.1016/j.ceramint.2021.08.032>
17. Chen Y, Wang N, Ola O, et al. (2021) Porous ceramics: Light in weight but heavy in energy and environment technologies. *Mater Sci Eng R* 143: 100589. <https://doi.org/10.1016/j.mser.2020.100589>
18. Çelik A, Çağlar G, Çelik Y (2022) Fabrication of porous Al<sub>2</sub>O<sub>3</sub> ceramics using carbon black as a pore forming agent by spark plasma sintering. *Ceram Int* 48: 28181–28190. <https://doi.org/10.1016/j.ceramint.2022.06.121>
19. Maurath J, Willenbacher N (2017) 3D printing of open-porous cellular ceramics with high specific strength. *J Eur Ceram Soc* 37: 4833–4842. <https://doi.org/10.1016/j.jeurceramsoc.2017.06.001>
20. Nuaklong P, Jongvivatsakul P, Pothisiri T, et al. (2020) Influence of rice husk ash on mechanical properties and fire resistance of recycled aggregate high-calcium fly ash geopolymer concrete. *J Clean Prod* 252: 119797. <https://doi.org/10.1016/j.jclepro.2019.119797>
21. Yang Y, Ma M, Zhang F, et al. (2020) Low-temperature sintering of Al<sub>2</sub>O<sub>3</sub> ceramics doped with 4CuO-TiO<sub>2</sub>-2Nb<sub>2</sub>O<sub>5</sub> composite oxide sintering aid. *J Eur Ceram Soc* 40: 5504–5510. <https://doi.org/10.1016/j.jeurceramsoc.2020.06.068>



AIMS Press

© 2023 the Author(s), licensee AIMS Press. This is an open access article distributed under the terms of the Creative Commons Attribution License (<http://creativecommons.org/licenses/by/4.0>)